

the precursors flowed into the heated section, where they quickly reacted to form NCs. The NC solution was then collected for absorption and photoluminescence measurements.

Optical absorption spectra were acquired using a Hewlett-Packard 8453 diode array spectrometer. Photoluminescence spectra were acquired using a SPEX Fluorolog 1680 spectrometer, using right-angle collection. Samples were prepared by diluting the raw NC solutions in hexane. Quantum yields were determined by comparing the integrated emission of a given NC sample solution with that of an appropriate reference dye [18].

Received: March 26, 2003

Final version: July 18, 2003

Published online: September 11, 2003

- [1] a) M. Bruchez Jr., M. Moronne, P. Gin, S. Weiss, A. P. Alivisatos, *Science* **1998**, *281*, 2013. b) W. C. W. Chan, S. Nie, *Science* **1998**, *281*, 2016. c) H. Mattoussi, J. M. Mauro, E. R. Goldman, G. P. Anderson, V. C. Sundar, F. V. Mikulec, M. G. Bawendi, *J. Am. Chem. Soc.* **2000**, *122*, 12 142.
- [2] a) V. L. Colvin, M. C. Schlamp, A. P. Alivisatos, *Nature* **1994**, *370*, 354. b) B. O. Dabbousi, M. G. Bawendi, O. Onitsuka, M. F. Rubner, *Appl. Phys. Lett.* **1995**, *66*, 1316. c) M. C. Schlamp, X. Peng, A. P. Alivisatos, *J. Appl. Phys.* **1997**, *82*, 5837. d) N. Tessler, V. Medvedev, M. Kazes, S. Kan, U. Banin, *Science* **2002**, *295*, 1506. e) S. Coe, W.-K. Woo, M. G. Bawendi, V. Bulovic, *Nature* **2002**, *420*, 800.
- [3] a) V. I. Klimov, A. A. Mikhailovsky, S. Xu, A. Malko, J. A. Hollingsworth, C. A. Leatherdale, H.-J. Eisler, M. G. Bawendi, *Science* **2000**, *290*, 314. b) M. Kazes, D. Y. Lewis, Y. Ebenstein, T. Mokari, U. Banin, *Adv. Mater.* **2002**, *14*, 317. c) V. C. Sundar, H.-J. Eisler, M. G. Bawendi, *Adv. Mater.* **2002**, *14*, 739. d) H.-J. Eisler, V. C. Sundar, M. G. Bawendi, M. Walsh, H. I. Smith, V. I. Klimov, *Appl. Phys. Lett.* **2002**, *80*, 4614. e) A. V. Malko, A. A. Mikhailovsky, M. A. Petruska, J. A. Hollingsworth, H. Htoon, M. G. Bawendi, V. I. Klimov, *Appl. Phys. Lett.* **2002**, *81*, 1303.
- [4] C. B. Murray, D. J. Norris, M. G. Bawendi, *J. Am. Chem. Soc.* **1993**, *115*, 8706.
- [5] a) C. B. Murray, S. Sun, W. Gaschler, H. Doyle, T. A. Betley, C. R. Kagan, *IBM J. Res. & Dev.* **2001**, *45*, 47. b) L. Qu, Z. A. Peng, X. Peng, *Nano Lett.* **2001**, *1*, 333. c) Z. A. Peng, X. Peng, *J. Am. Chem. Soc.* **2001**, *123*, 183. d) M. G. Bawendi, N. E. Stott, *US Patent 20 020 071 952*, **2002**.
- [6] X. Peng, J. Wickham, A. P. Alivisatos, *J. Am. Chem. Soc.* **1998**, *120*, 5343.
- [7] E. M. Chan, R. A. Mathies, A. P. Alivisatos, *Nano Lett.* **2003**, *3*, 199.
- [8] H. Nakamura, Y. Yamaguchi, M. Miyazaki, H. Maeda, M. Uehara, P. Mulvaney, *Chem. Commun.* **2002**, 2844.
- [9] J. B. Ediel, R. Fortt, J. C. deMello, A. J. deMello, *Chem. Commun.* **2002**, 1136.
- [10] a) H. Mattoussi, A. W. Cumming, C. B. Murray, M. G. Bawendi, R. Ober, *Phys. Rev. B* **1998**, *58*, 7850. b) M. K. Kuno, *Ph.D. Thesis*, Massachusetts Institute of Technology **1998**.
- [11] C. A. Leatherdale, W.-K. Woo, F. V. Mikulec, M. G. Bawendi, *J. Phys. Chem. B* **2002**, *106*, 7619. We have made the assumption that the number of dots is equal to the number of nuclei, which is true as long as growth does not proceed extensively by an Ostwald ripening mechanism. In Ostwald ripening, the concentration of monomers is low enough that smaller dots dissolve at the expense of larger dots, and we would observe a decrease in the number of dots with sufficiently long growth time. In all of the data presented here, the residence time was kept short enough so that this process did not occur.
- [12] See for example: a) M. A. Edadian, Z. F. Dong, in *Handbook of Heat Transfer* (Eds: W. M. Rohsenow, J. P. Harnett, Y. I. Cho), 3rd ed. McGraw Hill, New York **1998**, Ch. 5. b) J. R. Sellars, M. Tribus, J. S. Klein, *Trans. ASME* **1956**, *78*, 441. For our system, we estimated $0.1 \text{ W m}^{-1} \text{ K}^{-1}$, 0.9 g cm^{-3} , and $3 \text{ J g}^{-1} \text{ K}^{-1}$ for the fluid thermal conductivity, density, and heat capacity, respectively. We took as the boundary condition that the fluid at the channel wall is at a constant 25°C before the heated region and a constant 320°C within the heated region.
- [13] See, for example: a) H. S. Fogler, in *Elements of Chemical Reaction Engineering*, 3rd ed., Prentice Hall, Upper Saddle River, NJ **1999**. b) O. Levenspiel, in *Chemical Reaction Engineering*, 3rd ed., Wiley, New York **1999**. In this model, the extent of dispersion in residence times is characterized by a dispersion coefficient, $D^* = (u^2 R^2)/(48D)$, where R is the radius of the channel, u is the average flow velocity, and D is the diffusion coefficient. D was estimated using the Stokes-Einstein equation. The fluid viscosity was extrapolated from experimental values for squalane (U. G. Krahn, G. Luft, *J. Chem. Eng. Data* **1994**, *39*, 670) using a modified Arrhenius expression.
- [14] Introducing a segmented, rather than a homogeneous flow, into the reactor can reduce the dispersion in the RTD. In such an approach, the flow is

comprised of small, alternating segments of two different phases moving through the heated section. Each segment behaves essentially like a miniature stirred tank reactor, so that molecules within each segment experience a very uniform RTD. In a previous report on the preparation of CdSe NCs with a flow system [8], researchers used a segmented flow by introducing N_2 bubbles into the precursor stream, and they observed somewhat improved size distributions in comparison to the homogeneous flow case. We have observed similar results when a lower boiling solvent, di-*n*-octyl ether rather than squalane, is used. At temperatures greater than $\sim 280^\circ\text{C}$, the solvent boils within the heated section, forming alternating segments of gas and liquid within the channel. However, it was difficult to estimate the flow velocity of the fluid in the heated region due to the nature of the bubble formation. Experiments are underway to more controllably introduce a gas phase into the liquid precursor stream.

- [15] T. Sugimoto, *Adv. Colloid Interface Sci.* **1987**, *28*, 65.
- [16] D. V. Talapin, A. L. Rogach, M. Haase, H. Weller, *J. Phys. Chem. B* **2001**, *105*, 12 278.
- [17] Under some conditions, such as a very broad initial size distribution, it is possible for Ostwald ripening to lead to narrowing of the size distribution [16]. Such conditions were not present in the data shown here.
- [18] The following reference dyes (and quantum yields) were used: Rhodamine 560 chloride in basic ethanol (92%), Rhodamine 590 chloride in methanol (89%), Rhodamine 610 chloride in methanol (57%), and Rhodamine 640 perchlorate in methanol (100%).

1.3 μm to 1.55 μm Tunable Electroluminescence from PbSe Quantum Dots Embedded within an Organic Device**

By Jonathan S. Steckel, Seth Coe-Sullivan, Vladimir Bulović, and Moungi G. Bawendi*

We demonstrate large area (mm^2 in size) infrared electroluminescent devices using colloiddally grown PbSe quantum dots (QDs) in organic host materials. By changing the QD size the electroluminescence is tuned from $\lambda = 1.33$ to $1.56 \mu\text{m}$ with a full width at half maximum (FWHM) of $< 160 \text{ nm}$ ($< 0.11 \text{ eV}$). This represents only a portion of the accessible QD tuning range, as the lowest energy optical absorption peak of our PbSe solutions can be tuned from 1.1 eV (corresponding to wavelength $\lambda = 1.1 \mu\text{m}$ and 2.6 nm diameter QDs) to 0.56 eV ($\lambda = 2.2 \mu\text{m}$, 9.5 nm diameter). Our light emitting device fabrication combines the thin film processing techniques available to organic materials with the tunable optical properties of PbSe QDs. Formation of double heterojunction devices is enabled by material phase segregation during the spin-coating step. Such large area emitters in the near infrared have been

[*] Prof. M. G. Bawendi, J. S. Steckel
Department of Chemistry, Massachusetts Institute of Technology
77 Massachusetts Avenue
Cambridge, MA 02139 (USA)
E-mail: mgb@mit.edu
S. Coe-Sullivan, Prof. V. Bulović
Laboratory of Organic Optoelectronics
Department of Electrical Engineering and Computer Science
Massachusetts Institute of Technology
Cambridge, MA 02139 (USA)

[**] J. S. Steckel and S. Coe-Sullivan contributed equally to this work. We thank M. Frangillo for assistance with the high-resolution electron microscopy. This work was funded in part by the NSF-MRSEC program (DMR 0213282) and by the U.S. Army through the Institute for Soldier Nanotechnologies, under Contract DAAD-19-02-0002 with the U.S. Army Research Office.

identified as technologically useful for chemical spectroscopy and sensing, and could be incorporated into on-chip optoelectronic integrated circuits.

Advances in the colloidal synthesis of inorganic nanocrystal QDs^[1-4] have enabled the creation of a wide range of new nanostructured materials that led to the development of several emerging technologies. Inorganic nanocrystals have been used in efficient solar cells,^[5] light-emitting devices (LEDs),^[6-9] and photostable fluorescent tags in biological systems.^[10-12] In this work, we utilize our previous visible quantum-dot LED (QD-LED) structures with infrared emitting PbSe nanocrystals to create infrared QD-LEDs with tunable and narrowband emission.

Established technologies, such as inorganic LEDs, lasers, photodetectors, and modulators, have been developed and optimized in the near infrared (NIR) to address the needs of optical communications, chemical spectroscopy, and chemical sensing. These devices have high performance and long lifetimes, but the associated fabrication and material costs are high and therefore prohibitive for cost-constrained applications that require large-area devices. New device paradigms that use less expensive fabrication processes and materials would enable the more widespread use of active NIR optoelectronic devices. Molecular and polymeric organics are among the materials that, in principle, meet these criteria, but as yet they are not readily available with efficient tunable emission beyond the wavelength of $\lambda = 1 \mu\text{m}$, even when inorganic complexes are used as the emitter in doped organic structures.^[13,14] In this study we generate NIR electroluminescence (EL) using inorganic PbSe nanocrystals in solution processible organic structures. Although our reported efficiencies are low, the demonstrated QD-LEDs are controllably tuned across the NIR spectrum and have the potential to be further improved based on the high solution photoluminescence (PL) efficiencies of the starting materials and our previous studies^[6,7] of efficient CdSe QD-LEDs.

PbSe is a convenient choice for inorganic semiconductor QDs for NIR applications ($\lambda > 1 \mu\text{m}$), as the colloidal synthesis is reproducible and yields nanocrystals with narrow size distributions. In addition, the exciton Bohr radius is large (46 nm),^[15] leading to strong confinement of QD excitons throughout the synthetically accessible range of 2 nm to 10 nm (corresponding to absorption peaks $\lambda = 1.0 \mu\text{m}$ (1.2 eV) to $\lambda > 2.4 \mu\text{m}$ (<0.5 eV), respectively). Figure 1a shows typi-

cal absorption and emission spectra for $d_{\text{core}} = 5.0 \pm 0.5 \text{ nm}$ diameter PbSe QDs, while Figure 1b depicts an ordered layer of $d_{\text{core}} = 4.0 \pm 0.5 \text{ nm}$ diameter QDs imaged by high-resolution transmission electron microscopy (HRTEM), showing in the inset an enlarged view of the atomic planes from two QDs. The narrow lowest energy absorption peaks in Figure 2 demonstrate consistently narrow QD size distributions over the entire tuning range (0.56 to 1.1 eV). This is also reflected in

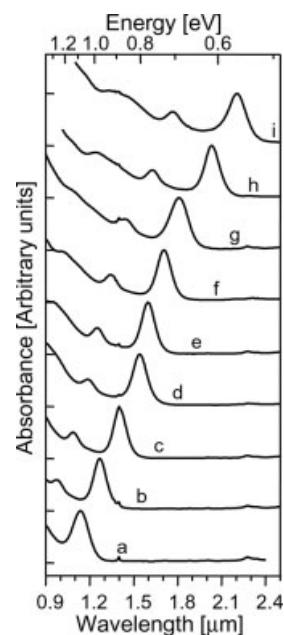


Fig. 2. Absorption spectra of a size series of PbSe nanocrystals ranging from 2.6 nm to 9.5 nm in diameter. The first absorption peaks (particle diameter) are for a) $\lambda = 1.14 \mu\text{m}$ ($d_{\text{CORE}} = 2.6 \text{ nm}$), b) $1.27 \mu\text{m}$ (3.7 nm), c) $1.40 \mu\text{m}$ (4.7 nm), d) $1.50 \mu\text{m}$ (5.2 nm), e) $1.60 \mu\text{m}$ (5.7 nm), f) $1.71 \mu\text{m}$ (6.2 nm), g) $1.81 \mu\text{m}$ (6.6 nm), h) $2.04 \mu\text{m}$ (7.6 nm), and i) $2.21 \mu\text{m}$ (9.5 nm). Core sizes were measured from TEM images such as in Figure 1b. The uncertainty in measuring the core diameters is $\pm 10 \%$.

the well-defined secondary absorption peaks corresponding to higher energy exciton states. The measured^[16] absolute PL efficiency (η_{PL}) of our PbSe QD solutions ranges from 6 to 20% and is reduced to 0.5 to 1.5% when the QDs are in a thin film, in contrast to relative η_{PL} of 10 to 80% for PbSe QDs in solution reported by others.^[17,18] The lack of convenient luminescent standards in the NIR spectral range could be responsible for the differences in quantum yield measurements reported in the literature.

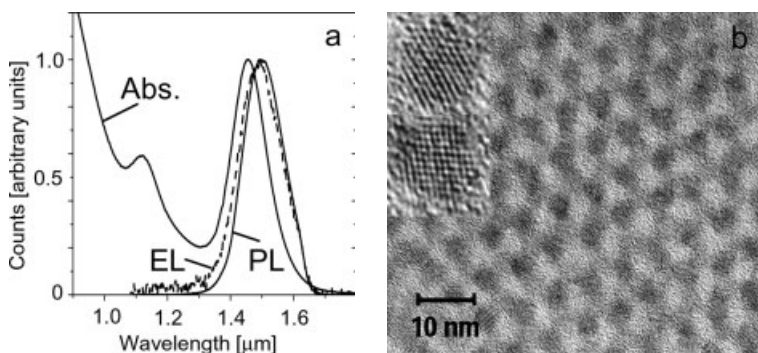


Fig. 1. a) Typical absorption (peak at $\lambda = 1.456 \mu\text{m}$), photoluminescence (peak at $\lambda = 1.500 \mu\text{m}$), and electroluminescence spectra (peak at $\lambda = 1.495 \mu\text{m}$) of $d_{\text{CORE}} = 5.0 \pm 0.5 \text{ nm}$ diameter PbSe particles; b) HRTEM image of $d_{\text{CORE}} = 4.0 \pm 0.5 \text{ nm}$ diameter PbSe particles with two enlarged images (inset).

Our basic synthetic scheme for the colloidal synthesis of PbSe QDs capped with oleic acid, briefly described by Murray and co-workers^[2] was optimized to yield consistently narrow QD size distributions throughout the size tuning range. A very clean sample of QDs is required if the characteristics of our devices are not to be dominated by impurities in the starting QD solution. To this end, care was taken at each processing step to remove any unreacted material, and to eliminate all reaction byproducts after QD growth. To inhibit the oxidation of the PbSe surface, the QDs are processed air-free, handled in anhydrous solvents, and are stored dry (solvent free) under a positive pressure of inert gas. Over a period of 14 days, surface oxidation of QDs in solution stored in the dark can both shift their PL maximum to shorter wavelengths by more than 100 nm and decrease η_{PL} by 30 to 50 % of the initial value. The decrease in η_{PL} is accelerated when oxygen is bubbled through a QD solution for 1 min immediately following synthesis or when the solution is stored in air, consistent with a surface oxidation process.

Device fabrication uses QDs processed air-free and dispersed in anhydrous chloroform in a nitrogen environment (<10 ppm O_2 and H_2O). The QD solution is added to a chloroform solution of a hole transporting organic semiconductor, N,N' -diphenyl- N,N' -bis(3-methylphenyl)-(1,1'-biphenyl)-4,4'-diamine (TPD) or 4,4-bis[N -(1-naphthyl)- N -phenylamino]biphenyl (α -NPD), and is spin cast onto a clean indium tin oxide (ITO) coated glass substrate. The QDs phase segregate into a monolayer (or sub-monolayer) on the surface of the organic film (shown in Fig. 3), as described previously.^[6,7] The substrate is then transported into a thermal evaporator without exposure to air where the electron-transporting layers (ETL), tris-(8-hydroxyquinoline)aluminum (Alq_3) and/or bathocuproine (BCP), are deposited at $<5 \times 10^{-6}$ torr. Finally, the metal cathode (50 nm thick Mg/Ag, 50:1 by weight, 50 nm Ag cap) is thermally evaporated through a shadow mask to define 1 mm diameter devices. The assembled device structure is shown in the inset of Figure 4a. High device yields and consistent LED performance are standard for devices fabricated in this manner.

Deposition of the hole-transport layer (HTL) and the QD monolayer relies on a phase segregation process during spin casting. Indeed, the phase segregation phenomenon could be a general technique for the formation of QD monolayers on organic thin film surfaces as it has been observed in spin cast solutions of (CdSe)ZnS core-shell/tri- n -octylphosphine oxide (TOPO) capped QDs^[6,7] and PbSe/oleic acid capped QDs (this work) with both NPD and TPD in chloroform and chlorobenzene. The narrow size distribution of our PbSe QDs yields hexagonally packed layers with domain sizes of the order of $10\,000\text{ nm}^2$ (~ 300 QDs per domain), as shown in Figure 3. QDs have a tendency to pack into regular hexagons, as seen in the incomplete monolayer of Figure 3b, minimizing the QD island perimeter while maximizing the interparticle van der Waals interactions. From the atomic force microscopy (AFM) image of Figure 3c we measure an average QD center-to-center distance of $d_{\text{ctoc}} = 6.5 \pm 0.5$ nm. For this QD sam-

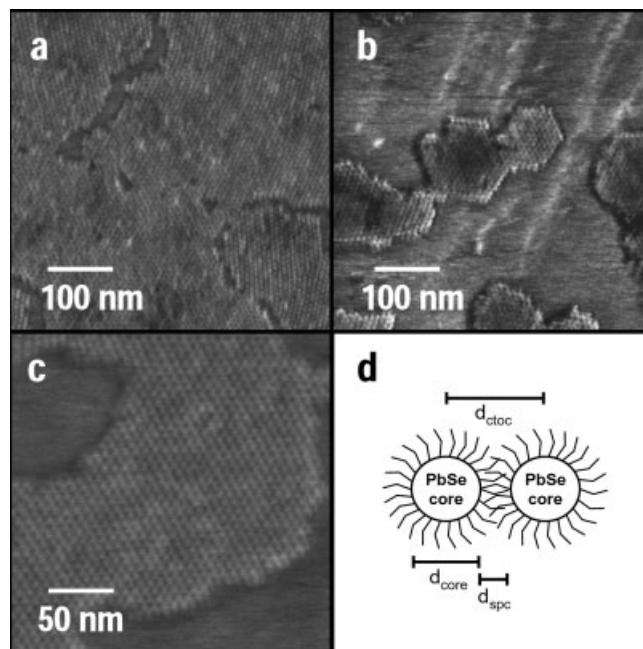


Fig. 3. AFM images of 5.0 ± 0.5 nm diameter PbSe QDs ordered on the surface of TPD. Image a) shows that close to full monolayer coverage can be achieved by varying the spin solution concentrations; b) demonstrates that for the narrowest size distributions of QDs, ordered formation of regular hexagons occurs; c) depicts a highly ordered, large domain of PbSe QDs, used to measure the average QD center-to-center distance; d) depicts two close packed QDs surrounded by oleic acid capping molecules, and the distances associated with such a packing geometry. d_{ctoc} is the QD center-to-center spacing, and is measured by AFM; d_{core} is the core diameter, measured by TEM; d_{spc} denotes the spacing distance between QDs, and is calculated as $d_{\text{ctoc}} - d_{\text{core}}$. Our experiments confirm that d_{spc} is less than twice the length of an oleic acid molecule, indicating that capping molecules on adjacent QDs interpenetrate each other.

ple, which has a lowest energy peak absorption at $\lambda = 1.4\ \mu\text{m}$, TEM measurements of drop cast films show a core diameter of $d_{\text{core}} = 4.7 \pm 0.4$ nm. Since the calculated length of fully extended oleic acid is 1.8 nm, the $d_{\text{spc}} = 1.8 \pm 0.6$ nm spacing between QDs is consistent with the interpenetration of oleic acid capping molecules on neighboring QDs (see Fig. 3d).

The NIR EL spectrum of QD-LEDs closely resembles the PL spectrum of the corresponding QD solution (see Fig. 1a). The tunability of QD-LED emission as a function of the QD diameter is shown in Figure 4a, with EL spectral peaks at $\lambda = 1.33\ \mu\text{m}$, $1.42\ \mu\text{m}$, $1.50\ \mu\text{m}$, and $1.56\ \mu\text{m}$. The spectral FWHM of all four devices is <160 nm (<0.11 eV). The devices also have an emission peak at $\lambda = 530$ nm (not shown) due to exciton recombination within the Alq_3 ETL (or $\lambda = 405$ nm corresponding to TPD EL when BCP is used as the ETL). We note that the InGaAs photodiode array used to record all of these spectra has a low detection efficiency for $\lambda > 1.6\ \mu\text{m}$, modifying the apparent shape of the $\lambda = 1.56\ \mu\text{m}$ emission peak.

The electrical characteristics of all the QD-LEDs of this study are similar, with a typical performance shown in Figure 4b. The current density (J) versus voltage (V) plot shows a linear dependence for $V < 3$ V, and power law dependence, $J \sim V^9$, when light is emitted. This is consistent with the properties of an Alq_3 /TPD device, though the operating voltage is

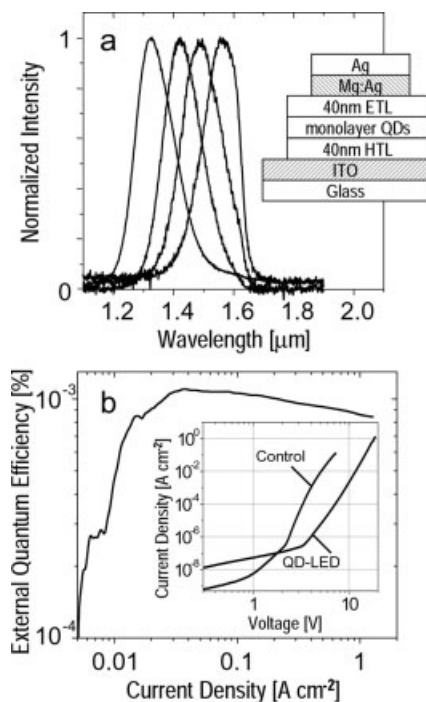


Fig. 4. a) Normalized electroluminescence spectra of a series of QD-LEDs tuned through the NIR (emission peaks at $\lambda = 1.33 \mu\text{m}$, $1.42 \mu\text{m}$, $1.50 \mu\text{m}$, and $1.56 \mu\text{m}$). The spectrum of the device emitting at $1.56 \mu\text{m}$ is asymmetric due to the quantum efficiency of the cooled InGaAs detector dropping from 90 % to below 10 % for $1.58 \mu\text{m} < \lambda < 1.62 \mu\text{m}$. The inset shows the general device structure for all of the QD-LEDs reported in this work. b) External quantum efficiency and current-voltage plots for a PbSe QD-LED. The peak external quantum efficiency of 0.001 % is obtained at 37 mA cm^{-2} and 13.3 V. The current-voltage characteristics are compared to a control device, which is identical in structure except that the QD monolayer is omitted. This comparison exemplifies the increase in operating voltage that is typical of QD-LEDs.

higher, possibly due to QD charge trapping, realignment of interface dipoles, or charge screening by QDs. The PbSe QD-LED NIR external quantum efficiency (η_{EL}) is measured to be 0.001 %, using a silicon wafer to filter out visible emission from organic EL. The visible emission originates from Alq₃ and TPD (when BCP is used as the ETL) and has an external EL quantum efficiency of 0.1–0.3%. These QD-LEDs demonstrate the feasibility of generating controllably tunable $\lambda > 1.3 \mu\text{m}$ EL in a large area device, and give us a starting point in the creation of higher efficiency devices. Based on the absorption spectra shown in Figure 2, we conclude that this device platform could be used to generate devices emitting in the spectral range of $1.2 \mu\text{m} < \lambda < 2.2 \mu\text{m}$ (measurement of our EL spectra are limited to $\lambda < 1.6 \mu\text{m}$ due to the detector cut-off).

The low η_{EL} of our devices is the result of the lowered quantum efficiency of films of close packed QDs and a device design that is optimized for visible emission. While PbSe QDs have been shown to be very efficient NIR emitters in solution, the η_{PL} drops to 0.5 to 1.5 % in thin film form. This is due to a reduction in the number of available capping molecules to the QDs in thin film form, as well as exciton energy transfer within the QD film, both of which have been shown to reduce η_{PL} in QD solids. Extrapolating from other QD material systems,

it is reasonable to assume that the development of a core-shell PbSe QD would result in higher solid state η_{PL} . Our active layer thickness and choice of organic semiconductors was originally designed for visible emitting organic LEDs. For the long wavelength devices described in this paper, the optical mode overlap with the emissive QD layer is poor. Designs using a transparent highly conductive cathode would allow optimization of the distance between the metal and the emissive QD monolayer without incurring an increase in the operating voltage.^[19,20] We further note that the choice of ITO as the anode in our devices is not ideal, since the transparency of the 150 nm film is only 70 % at $\lambda = 1.5 \mu\text{m}$.

Previous work has suggested that Förster energy transfer and direct charge injection are both potential mechanisms for QD excitation within QD-LEDs.^[7] (We find that radiative excitation of the QDs by green Alq₃ EL (spectral peak at $\lambda = 530 \text{ nm}$) is a negligible source of QD-NIR emission.^[21]) Exciton energy transfer should be possible for excitons created in the organic layer close to QDs despite the large capping group length ($\sim 1.8 \text{ nm}$). In contrast, photoconductivity experiments indicate that the 1.8 nm tunnel barrier is sufficient to reduce direct injection of charge carriers from the semiconducting organics into the QD core by several orders of magnitude relative to a QD capped with a shorter chain capping molecule.^[22] For both mechanisms, however, shorter chain capping groups would serve to increase the likelihood of QD excitation. If we assume a Förster energy transfer process, the energy of the transferred exciton from Alq₃ molecules to QDs would initially be 2.4 eV (corresponding to the excited state of Alq₃). The generated QD exciton would then lose $\sim 1.6 \text{ eV}$ before occupying the lowest energy state, from which QD emission originates. Since PbSe QD η_{PL} is constant over a wide range of excitation wavelengths, PbSe QD-LEDs with higher power efficiency could be realized if organic transport materials with smaller optical gaps were utilized.

To accurately measure the efficiency and the EL spectrum of QD-LEDs it is necessary to maximize the detected NIR emission and attenuate the emission signal of both organic and blackbody radiation by using appropriate spectral filters, detectors, and detection geometry.^[23] In our quantum efficiency measurements, the NIR signal (1–50 nW) is maximized using a minimum distance between the emitter and a large area detector (3 mm distance, 3 mm diameter Newport 818-IR-C/M germanium detector). The spectral measurements were performed using an InGaAs photodiode array cooled to 173 K (Roper Scientific OMA V) and monochromator with a fiber bundle input. The fiber bundle was coupled to the device substrate to maximize the input signal. For both efficiency and spectral measurements, the visible emission is filtered out using a double sided polished, 500 μm thick, silicon wafer. The three lowest order diffraction peaks of Alq₃ (at $\lambda = 530 \text{ nm}$, 1060 nm, and 1590 nm) that are otherwise detected by the spectrograph are completely eliminated when the Si filter is in place. Finally, the possible detection of blackbody radiation must be accounted for. Our 1 mm diameter devices were run at currents as high as 10 mA and 20 V oper-

ating voltages, corresponding to 200 mW of peak input electrical power. The power efficiency of these devices is no better than 0.1 %, implying that 99.9 % of the input power is converted to heat.^[24] While a large portion of this heat will be lost to the surrounding air by conduction and convection processes, there is no doubt that some device and substrate heating to above room temperature does occur. Blackbody radiation at 300 K to 350 K has the bulk of its emission in the $\lambda = 17 \mu\text{m}$ range, but a measurable quantity of emission is in the $\lambda = 1.1 \mu\text{m}$ to $1.7 \mu\text{m}$ detection window of Ge and InGaAs detectors. Our actual detected power in this spectral window was in all cases greater than 1 nW. A temperature rise of 70 °C over the 150 mm² area of our substrates would be required to generate 1 nW of power in the spectral detection window. Our device could not support such a rise as the glass transition temperature of TPD is 65 °C.^[25] Furthermore, substrate inspection indicates that QD-LEDs are not warm to the touch during operation. A temperature rise of less than 10 °C corresponds to <20 pW of detectable radiated power, and thus a <2% error in measurement of QD-LED NIR η_{EL} . This analysis shows that the detected power is therefore not a result of either blackbody radiation or visible organic EL, and is in fact due to the band edge emission from the QDs.

In conclusion, we demonstrate large area NIR EL from QD-LEDs. The LED emission is tuned from $\lambda = 1.32$ to $1.56 \mu\text{m}$ as the PbSe QD diameter is changed from $d_{\text{core}} = 4$ to 5 nm, without any modification to the device structure. Processing of the colloiddally grown semiconductor QDs and the organic small molecules from the same solvent allows for the simple fabrication of double heterojunction devices, where the NIR emissive layer is only one monolayer thick. Using CdSe QD-LEDs as a model, we expect significant improvement of PbSe QD-LED performance through both device engineering and chemical optimization of the materials.

Experimental

The PbSe nanocrystals are synthesized by injecting a 5 mL solution of 1 M tri-*n*-octylphosphine selenide into a round bottom flask containing degassed diphenylether (15–25 mL), oleic acid (1–2 mmol), and lead(II) acetate trihydrate (1 mmol), stirred under argon, at a temperature of 100–180 °C. After injection, the nucleated particles are grown for 0–5 min. The synthesis is optimized to give narrow size distributions without further size processing. Different sizes are obtained by changing the injection temperature, the growth time, and the concentration of precursors in the solution. The yield is typically 10–30 % and the particle size distribution has a standard deviation (σ) of ~5–8 %. Oleic acid is the capping group, as confirmed by ¹H NMR. In place of the high-melting point solvent (~26.8 °C) diphenylether, squalene, dioctylether, or tri-*n*-octylphosphine, which are liquids at room temperature, can also be used. For example, direct substitution of squalene for diphenylether yields larger diameter particles, with very narrow size distributions. After the reaction is complete anhydrous methanol is added to the growth solution under an inert atmosphere and the particles are isolated via centrifugation. They are then redispersed in anhydrous trichlorotrifluoroethane and precipitated once more with anhydrous methanol.

After centrifugation the nanocrystals are rinsed with anhydrous methanol and any excess solvents left behind are removed using vacuum.

Received: May 27, 2003
Final version: August 5, 2003

- [1] B. O. Dabbousi, J. Rodriguez-Viejo, F. V. Mikulec, J. R. Heine, H. Mattoussi, R. Ober, K. F. Jensen, M. G. Bawendi, *J. Phys. Chem. B* **1997**, *101*, 9463.
- [2] F. Chen, K. L. Stokes, W. Zhou, J. Frang, C. B. Murray, *Mater. Res. Soc. Symp. Proc.* **2001**, *691*, G10.2.
- [3] Y. W. Cao, U. Banin, *J. Am. Chem. Soc.* **2000**, *122*, 9692.
- [4] D. Battaglia, X. Peng, *Nano Lett.* **2002**, *2*, 1027.
- [5] W. U. Huynh, J. J. Dittmer, P. A. Alivisatos, *Science* **2002**, *295*, 2425.
- [6] S. Coe-Sullivan, W. K. Woo, M. Bawendi, V. Bulović, *Nature* **2002**, *420*, 800.
- [7] S. Coe-Sullivan, W. K. Woo, J. S. Steckel, M. G. Bawendi, V. Bulović, *Org. Electron.*, in press.
- [8] N. Tessler, V. Medvedev, M. Kazes, S. H. Kan, U. Banin, *Science* **2002**, *295*, 1506.
- [9] L. Bakueva, S. Musikhin, M. A. Hines, T. W. F. Chang, M. Tzolov, G. D. Scholes, E. H. Sargent, *Appl. Phys. Lett.* **2003**, *82*, 2895.
- [10] M. Bruchez, Jr., M. Moronne, P. Gin, S. Weiss, P. A. Alivisatos, *Science* **1998**, *281*, 2013.
- [11] W. C. W. Chan, S. Nie, *Science* **1998**, *281*, 2016.
- [12] H. Mattoussi, J. M. Mauro, E. R. Goldman, G. P. Anderson, V. C. Sundar, F. V. Mikulec, M. G. Bawendi, *J. Am. Chem. Soc.* **2000**, *122*, 12 142.
- [13] R. J. Curry, W. P. Gillin, A. P. Knights, R. Gwilliam, *Opt. Mater.* **2001**, *17*, 161.
- [14] Y. Kawamura, Y. Wada, M. Iwamuro, T. Kitamura, S. Yanagida, *Chem. Lett.* **2000**, 280.
- [15] F. W. Wise, *Acc. Chem. Res.* **2000**, *33*, 773.
- [16] Absolute PL quantum efficiency in both the solution and solid state was measured using a $\lambda = 405 \text{ nm}$ laser as the excitation source. The absorbed power was quantified using a Newport 818-UV-C/M silicon detector. The NIR signal was detected 15° off of the front face normal, 10 cm distant from the sample, with a silicon filter in place to block all reflected visible emission. The solid angle bisected by the 3 mm diameter germanium detector was taken into account when calculating the total NIR emission. The solution samples were measured in a 2 mm path length quartz cuvette, and the solid state samples were measured from drop-cast films that were isolated from oxygen to prevent photo-oxidation during the measurement. Relative PL quantum yield experiments reveal no dependence on excitation wavelength throughout the analyzed range of $\lambda = 400$ to 900 nm.
- [17] H. Du, C. Chen, R. Krishnan, T. D. Krauss, J. M. Harbold, F. W. Wise, M. G. Thomas, J. Silcox, *Nano Lett.* **2002**, *2*, 1321.
- [18] B. L. Wehrenberg, C. Wang, P. Guyot-Sionnest, *J. Phys. Chem. B* **2002**, *106*, 10 634.
- [19] V. Bulović, V. B. Khalfin, G. Gu, P. E. Burrows, *Phys. Rev. B* **1998**, *58*, 3730.
- [20] R. R. Chance, A. Prock, R. Silbey, *J. Chem. Phys.* **1974**, *60*, 2744.
- [21] A $\lambda = 532 \text{ nm}$ laser was used to excite a 1 mm spot on the device substrate, and its infrared emission monitored using a germanium detector with a 500 μm thick silicon wafer filter. The laser power was adjusted using neutral density filters to match the green optical power emitted by our device at its maximum brightness operating point, 10 μW . No optical signal was detected, allowing us to conclude that the Si filter effectively eliminates all trace of the Alq₃ emission from our EL device, and that the radiative excitation of the QDs from this Alq₃ emission is not sufficient to account for the measured NIR signal.
- [22] C. A. Leatherdale, C. R. Kagan, N. Y. Morgan, S. A. Empedocles, M. A. Kastner, M. G. Bawendi, *Phys. Rev. B* **2000**, *62*, 2669.
- [23] S. R. Forrest, D. D. C. Bradley, M. E. Thompson, *Adv. Mater.* **2003**, *15*, 1043.
- [24] J. C. Sturm, W. Wilson, M. Iodice, *IEEE J. Sel. Top. Quantum Electron.* **1998**, *4*, 75.
- [25] D. F. O'Brien, P. E. Burrows, S. R. Forrest, B. E. Koene, D. E. Loy, M. E. Thompson, *Adv. Mater.* **1998**, *10*, 1108.